Solar powered adsorption desalination for Northern and Southern Europe

Solar powered adsorption desalination for Northern and Southern Europe

Christopher Olkis[a], *Shihab AL-Hasni*[a], *Stefano Brandani*[a], *Salvatore Vasta*[b], *Giulio Santori*[a]

[a] *The University of Edinburgh, School of Engineering, Institute for Materials and Processes, Sanderson Building, The King's Buildings, Mayfield Road, EH9 3FB Edinburgh, Scotland, UK*
[b] *Institute CNR-ITAE, Via Salita S. Lucia Sopra Contesse 39, I-98126, Messina, Italy*

Abstract: Adsorption desalinators can be powered by solar energy to provide potable water and to mitigate increasing water stress throughout Europe. In this study, we analyse the feasibility of a solar powered adsorption desalination system design to produce drinking water at two distinct European locations, representing two extremes in terms of solar radiation. Detailed solar radiation data is used as input to an experimentally validated adsorption desalination model. The experimental validation is performed using advanced ionogel materials, as these materials show outstanding performance with regeneration temperatures as low as 25 °C. The system size requirements for the adsorption beds and solar collector area are calculated for each location and season. In Scotland, the system is viable for summer and spring, which tend to be the driest months. In Sicily, solar radiation is sufficient throughout the year and a system would require 140 kg of ionogel and 200 m^2 of solar collector area to produce one cubic metre of drinking water per day.

Keywords: *Adsorption desalination, low-grade-heat recovery, solar radiation, flat plate solar collector, ionogel*

1. Introduction

Unlike Southern Europe, Northern Europe is not commonly associated with drought conditions by the public. However, even Northern Europe is facing challenges of wet winters and dryer summers [1], which will only increase due to global warming [2]. Orth et al. report that the summer of 2015 was the driest on record in Central Europe and that models predict increasingly dryer summer seasons in the 21st century [3]. Pedro-Monzonis et al. [4] showed in a review of water and drought indices that some regions on the east coast of the UK suffer very high levels of water stress, which are comparable to southern Spain or Italy. Currently, there is only one large desalination plant operational in the UK, which supplies London with up to 150 million litres per day during dry periods and is expected to increase capacity by another 100 million litres per day by 2045 [5]. The plant's current electricity demand is 512.2 GWh per year [6], which will increase as a consequence of the increase in the capacity to 854 GWh per year. At the current UK emission factor [7], this plant is emitting 0.13 Mt of carbon dioxide per year and could emit up to 0.22 Mt of carbon dioxide in the near future. The seasonal concurrence of high water demand, dry periods and stronger solar radiation makes solar powered desalination an interesting solution [8]. Conventional desalination systems can use solar energy indirectly by converting it to electricity for Reverse Osmosis via photovoltaic solar panels that have up to 22 % efficiencies [9]. Advanced solar collectors show up to 80 % [10] thermal efficiencies for converting solar energy into thermal energy which can be used to power thermal desalination technologies.

The most efficient thermal desalination systems are Multi Stage Flash (MSF) and Multi Effect Distillation (MED) [11], which require 53-70 $kWh_{th}\ m^{-3}$ and 40-65 $kWh_{th}\ m^{-3}$ of low-grade heat, respectively [12]. In comparison Reverse Osmosis has an electricity demand of 2-4 $kWh_{el}\ m^{-3}$ [13]. Despite their seemingly higher energy demand, solar powered thermal desalination systems are favourable over membrane systems in terms of cost [13]. The cost of water from Reverse Osmosis powered by photovoltaics is reported at 11-15 Euro m^{-3} [14], while an MED plant driven by concentrated solar power is estimated at 2-3 Euro m^{-3}.

Thermal desalination systems are usually driven by industrial waste heat, but pilot plants of the two technologies have been operated with solar energy [8]. El-Nashar et al. have presented a long-term study on a MED system powered by a 1862 m^2 solar field [15] and Moustafa et al. presented a MSF pilot plant powered by a 220 m^2 solar collectors [16].

Beyond the established commercial desalination technologies, adsorption desalination represents an emerging desalination method [17,18], which evolved from adsorption chillers [19,20]. The main advantage of desalination by means of sorption cycles is the possibility of using low-grade heat at ultralow temperature levels [21] that other thermally-driven technologies cannot exploit. Sorption desalination has been proven at temperatures of only 5°C above ambient [22] and can operate without issues at temperatures <50°C using conventional sorption materials [23]. Studies have explored solar powered adsorption ice makers [24,25], refrigerators [26,27] and air conditioners [28,29]. Recently, experimental solar powered adsorption desalinators have been introduced as well. Alsaman et al. presented an experimental adsorption desalinator, where 13.5 kg of adsorption material was powered by a 4.5 m^2 evacuated tube solar collector in Egypt [30]. Moreover, Kim et al. analysed the water quality of a solar powered experimental adsorption desalinator [31]. Their results showed that the water quality is comparable to deionised water [31]. Du et al. estimated the lowest unit operation cost to produce fresh water from a solar powered adsorption desalinator for three different Chinese regions [32]. Their analysis was based on energy efficiency estimations of different system configurations they obtained from the literature. Results indicated that a conventional adsorption desalinator could produce water at a cost of 10-15 Euro m^{-3} [32]. However, their study neither presented a specific system design nor specified an adsorption material. The adsorption material is important as it enables the amount of water produced to be defined for a given system size, which is expressed through the Specific Daily Water Production (SDWP). Most current systems rely on silica gel, which requires temperatures above 70 °C for optimal regeneration to achieve an SDWP of about 10 m^3 of water per tonne of silica gel per day [17].
The development of advanced adsorption materials is crucial for increased performance and reduced costs as they enable larger water uptake capacities and faster cycle times leading to higher SDWP than silica gel. Here, metal organic frameworks [18,33] and ionogels [21,34,35] have received recent attention. A higher SDWP would allow smaller adsorption desalinators to produce the same amount of water, thus reducing costs significantly. A previous experimental study has shown that novel ionogel materials can outperform silica gel with an SDWP of up to 18 m^3 of water per tonne and day at regeneration temperatures below 45 °C [22]. Hence, an adsorption desalinator using ionogels would require half the adsorption bed size of a silica gel system.
There remains a need to further develop the concept of solar powered adsorption desalination from experimental studies to a more detailed analysis towards a commercial product. So far, studies have explored adsorption desalination as a process driven by industrial waste heat, which reduces adsorption desalination to an add-on process depended on existing plants. Solar powered adsorption desalination proposes the process as a standalone solution to mitigate water stress.
This study explores the feasibility of a solar powered adsorption desalinator in the UK and Italy using experimentally validated dynamic simulations. The two locations represent two extreme cases for Europe with very high solar radiation in southern Italy, which is representative for all Mediterranean countries, whereas solar radiation in the north of the UK is comparably low. Highly detailed, experimental solar radiation data is used for both locations.
The two locations represent both ends of the scale, almost all other European locations fall in between these in terms of solar intensity. Solar radiation data is used as heat input to an adsorption desalinator in a dynamic simulation. The adsorption desalination model is validated against experimental data from a small adsorption desalinator using novel ionogel adsorption material. High latitudes are usually not economically viable for solar thermal desalination technologies, but materials such as ionogels that can be regenerated at temperatures below 50°C can enable the utilization of such technology also in apparently adverse climates. This is the first time a dynamic adsorption model is validated against ionogel. The dynamic simulations are used to estimate adsorption bed and solar collector areas per cubic metre of water. In addition, the analysis estimates the number of consumers that can be supplied by the system.

2. System description

The system design features an evacuated flat plate solar collector that is tilted towards the sun to provide thermal energy to heat up the top layer of a hot water tank. The upper layer of the hot water tank is connected to the adsorbers during desorption, thus driving the system. After flowing through the adsorber heat exchangers the water is returned to the third layer of the hot water tank. Moreover, the hot water tank acts as a sensible heat storage to enable water production during day and night. An external heat sink supplies cooling water at ambient temperature to the condenser and the adsorber for adsorption. The operation of an adsorption chiller as well as the system used for experimental validation are described in detail elsewhere [36,37].

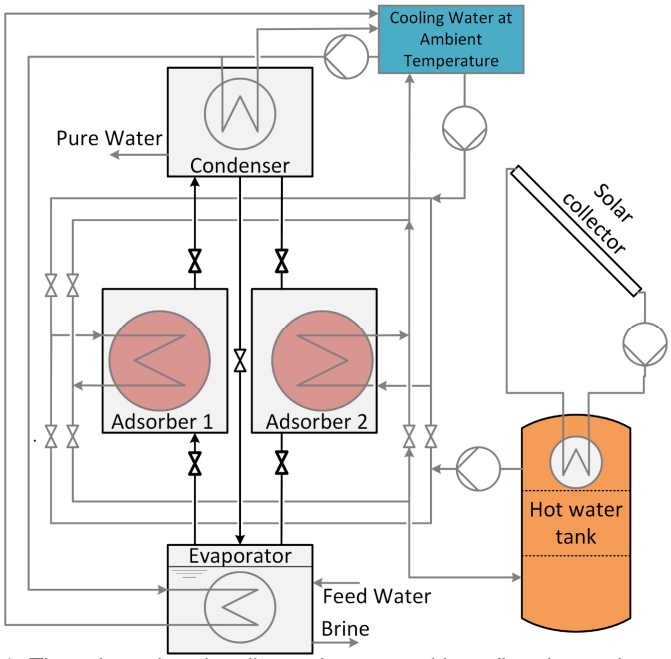

Figure 1: The adsorption desalinator is powered by a flat plate solar collector.

The modelling equations are given in the Appendix and the model assumes:

- Adiabatic hot water tank, piping and adsorption desalination vessels, while heat losses from the solar collector are considered;
- Homogeneous temperatures in vessels, the adsorption bed and within the three water layers of the hot water tank;
- A heat sink supplies cooling water at ambient temperature from climatic data to the condenser and adsorption beds. Heat losses from the solar collector are assessed by using the same ambient temperature. The ambient temperature was averaged by using the same process applied to the radiation data;
- Only pure water evaporates, while all salt remains in the evaporator [38].

2.1. Experimental solar radiation in Scotland and Sicily

Minute-by-minute diffuse and global solar radiation data measured at the University of Edinburgh (Scotland) in 2016 on the horizontal plane was provided by a Vaisala WXT520 weather station (Meter Group Inc., USA) modified with a Delta-T Devices BF5 sunshine sensor (AT Delta-T Devices Ltd, UK). Data were logged by using a Campbell Scientific CR1000 data logger (Campbell Scientific Ltd, UK). The measurement range is up to 1250 W m^{-2}, with an accuracy of ± 5 W m^{-2} on the global radiation and ± 20 W m^{-2} on the diffuse radiation. Global radiation measured on the horizontal plane was recorded by a weather station (SIAP+MICROS S.p.a., Italy) every 10 minutes for the year 2018 at CNR-ITAE in Messina (Italy). This weather station consists of a pyranometer, a combined wind speed and

direction transducer, an air temperature transducer, an air R.H. transducer and a digital barometer. In particular, the pyranometer measures the global solar radiation, calculated as sum of the direct sun radiation and the radiation diffused by the sky and scattered clouds. The measurement range is up to 1300 W m^{-2}, with an accuracy of ± 10 W m^{-2}. All the measured data are continuously recorded by an e020 MicroDA data-logger (SIAP+MICROS S.p.a., Italy) managing remote telemetry.
Both weather stations acquire radiation on the horizontal plane. The latitude ϕ for Edinburgh is 55.95°N and Messina's is 38.19°N. The two European locations represent two extreme cases within Europe, whereas Messina is blessed with some of Europe's highest solar radiation, Scotland is the other extreme with comparably low solar radiation and a colder climate. The vast majority of Europe's population lives within the latitudes of Messina and Edinburgh. Hence, a system design that is viable for the two locations can be used throughout Europe and the Mediterranean basin.
The data of one year was processed to generate an average day for each season following the same approach used in [26]. Average days reduce the simulation times of the solar powered adsorption desalination model significantly, as the raw data is real weather data including longer periods of sunny and cloudy days. Hence, the dynamic simulations would have to input long periods of raw data to generate an average performance if raw weather data were used.

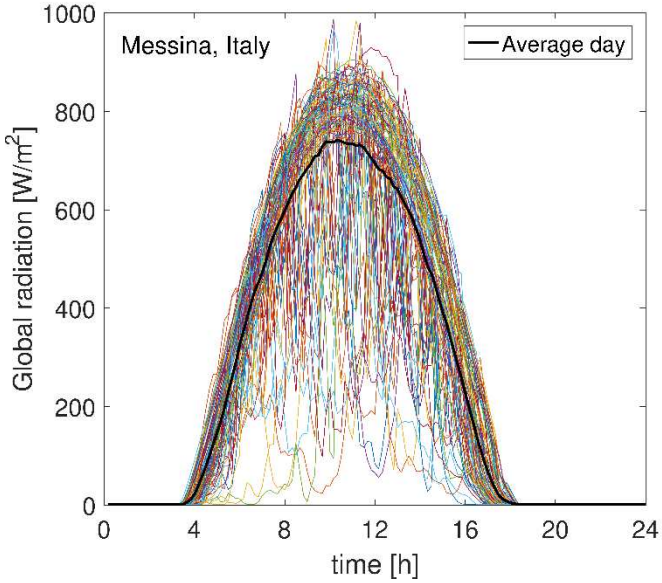

Figure 2: All days of June, July and August from experimental data for 2018 are plotted and used to generate an average summer day.

Solar radiation can be increased, when the horizontal plane is tilted south towards the sun [39]. In Fig. 3, the average days of the four seasons were tilted from 0° to 90° to find the optimal tilt for each season and to take an average value reflecting the optimal tilt for all seasons. Based on this analysis and the experimental data, the optimal tilt for Sicily is 43° for all seasons and 52° for Scotland. Both tilt angles are close to the latitude of the two locations, which is a guidance value for the tilting angle [40].

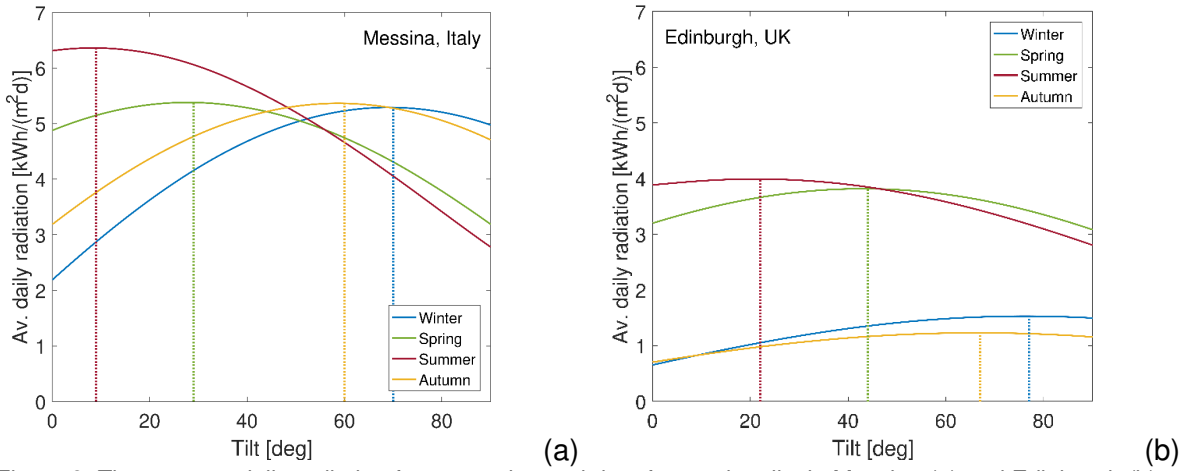

Figure 3: The average daily radiation from experimental data for varying tilts in Messina (a) and Edinburgh (b), where the mean optimal tilt for all seasons is 43° in Messina and 52° in Edinburgh.

Fig. 4 compares the radiation of the horizontal plane to the optimally tilted plane for Sicily and Scotland. In Sicily, the tilting angle slightly reduces the radiation on the solar collector in summer, but it almost doubles in autumn and winter. Overall, the tilted plane collects an almost constant peak of 600-700 W m^{-2} throughout all seasons.
In Edinburgh, the tilted plane can also improve the solar radiation in winter and autumn by a factor of 2-3 (Fig. 4b). However, in absolute values the peak radiation is only 300 W m^{-2} in autumn and winter. In summer, the tilted plane can only marginally improve the solar radiation, but it remains well below Sicily at 400-600 W m^{-2}.

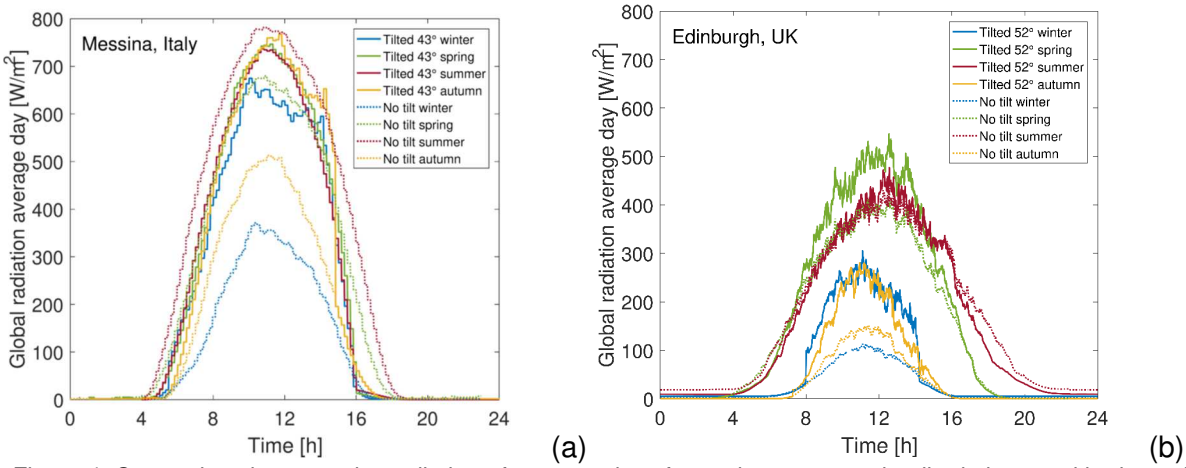

Figure 4: Comparison between the radiation of average days for each season on the tilted plane and horizontal plane for Messina (a) and Edinburgh (b).

3. Experimental calibration of the adsorption desalination model

The adsorption desalination model is presented in the appendix and was calibrated as part of this study against experimental results from a previous publication [22]. Results obtained using the small scale experimental heat transformer [36] are fully detailed elsewhere, [22,34,37,41] including heat transfer coefficients used as fitting parameters. The fitting results are given in Table 1. Experiments were performed with one partially filled heat exchanger containing 25 g of ionogel to assess the SDWP of the system. The SDWP is a performance indicator relative to the mass of the adsorption material.
The ionogel considered in this study is a composite material made of 50%wt 1-Ethyl-3-methylimidazolium acetate ionic liquid on Syloid 72FP silica gel. Equilibrium properties of the ionogel and hydrothermal stability have been extensively investigated in [22,34,35]. The Dubinin-Astakhov isotherm parameters can be found in Table A.3 of the appendix. Fig. 5

reports the isotherms and the differential enthalpy of adsorption as calculated from the isotherm parameters.

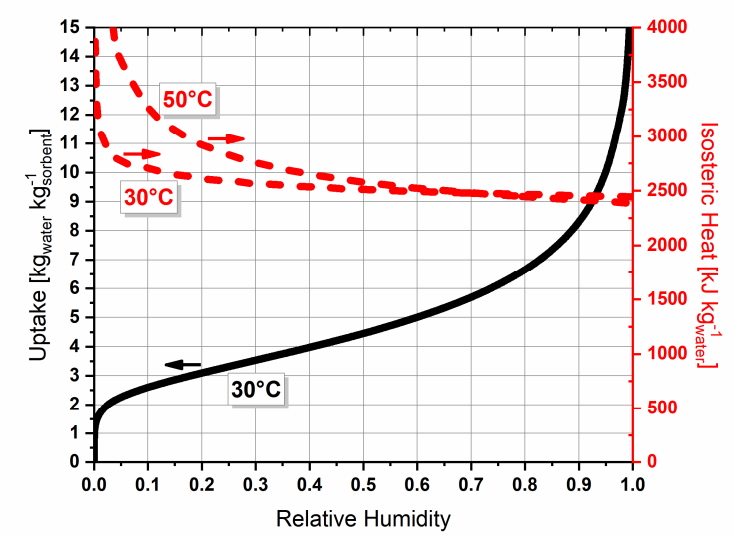

Figure 5: Isotherm at 30°C of the ionogel used in this study with corresponding isosteric heat of adsorption at 30°C and 50°C.

SDWP remains constant when the amount of adsorption material is increased from 25 g to 200 g. However, for the energy efficiency, the scale up of the adsorption material was necessary as the experimental system has aluminium heat exchangers of 600g each. Hence, the energy consumption of the heat exchanger at cyclic heating and cooling outweighs the water production using 25 g of ionogel leading to a poor energy performance. The same experimental system was previously operated with 200 g of silica gel [36] resulting in experimental performance ratios PR_{exp} up to 0.6, while with 25 g of ionogel led to PR_{exp} of 0.1, because of the weight of the aluminium heat exchangers. A system with such a low PR would require large solar collectors. The objective of the scale up was therefore to increase the PR by increasing the heat exchanger to ionogel mass ratio to 3, to make it comparable to the silica gel experiments. In addition, the heat transfer limitations of the experimental systems were reduced in the scaled-up model by increasing the flow rates of the heat exchangers by a factor of five, resulting in higher heat transfer coefficients as given in table 1. For the 25 g of ionogel (ig) experiments, the heat exchangers were partially filled with ionogel using 20 out of 125 channels. Thus, the heat transfer area increases by a factor of six compared for the completely filled heat exchanger. The factor of six is also reflected in UA_{ads} in table 1. Overall, the two models provide an excellent fitting of the experimental SDWP well in Fig. 5b.

Table 1: Fitting parameters for the adsorption desalination model scaled-up from 25g to 200g of ionogel (ig)

	25 g_{ig}	**200 g_{ig}**
UA_{ads} [W K^{-1}]	4	30
UA_{evap} [W K^{-1}]	6	70
UA_{cond} [W K^{-1}]	29	90
UA_{hx} [W K^{-1}]	25	90

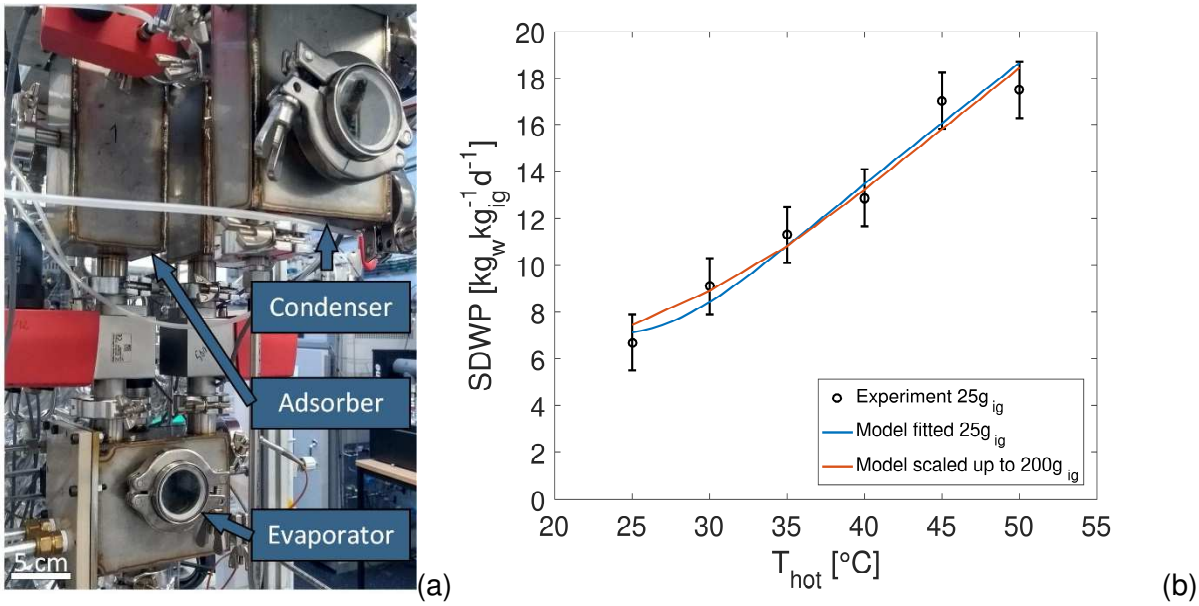

Figure 6: (a) The experimental system used for model calibration. (b) The adsorption desalination model was fitted to experimental data [22].

4. Results of the solar adsorption desalination model for Italy

The system is built of three main components: the tilted flat plate solar collector, sensible heat storage tank discretised in three layers and the desalinator. The sun heats up the surface of the solar collector. The average daily radiation and ambient temperature in summer are used as inputs to the equations system (Fig. 7). This heat is extracted by a cooling water system and stored in an insulated water tank as sensible heat. The water tank is modelled in three layers of water to account for a temperature gradient within the tank. Water from the hot water tank is used during desorption to heat the adsorption beds. A preliminary analysis tested the impact of the solar tank size on the system performance. The system was simulated with three different solar tank sizes of 100 L, 200 L and 300 L as sensible heat storage. The results showed that the performance is independent of the solar tank size as a smaller water tank leads to higher temperatures during the day resulting in a higher distillate output during the day, while a large water tank provides less fluctuating temperatures and a more even performance throughout the day.

From Fig. 7, it can be seen that the water temperature of the tank peaks in the late afternoon and reaches a minimum each day before sunrise. Hence, the water supplied to the adsorption beds changes in temperature during the day. The model runs with the parameters reported in Appendix (Table A.3). For Messina (Italy), the trend of the varying temperatures from Fig. 7a is reflected in Fig. 7c, which shows cycling heating and cooling of the adsorption beds. Fig. 7a also presents the predicted temperatures of the adsorption material inside the heat exchangers. The model suggests that the heat exchangers themselves undergo a large temperature gradient, but the adsorption material changes by less than 10 K during each cycle.

Experimental results have shown that a temperature difference of 5 K between adsorption and desorption achieves SDWP = 6.7 $kg_{water}\,kg_{ig}^{-1}\,day^{-1}$ [22]. From Fig. 7, it can also be seen that cycling continues overnight, because the hot water tank can store enough thermal energy to continue powering the process. The adsorber works within an average relative humidity swing between 15% and 25% centred in an average that varies across the day between 40% and 65%. The comparison between the uptake in Figure 7b and the isotherm in Fig. 5 shows that the ionogel never achieves the equilibrium uptakes.

The main performance indicators in adsorption desalination are the Specific Daily Water Production *SDWP* [$kg_{water}\,kg_{ig}^{-1}\,day^{-1}$], Performance Ratio *PR* [-] and Specific Energy consumption *SEC* [kWh m_{water}^{-1}]:

$$SDWP = \int_0^t \frac{\dot{Q}_{cond}}{L_w \cdot M_{sg}} dt \quad (1)$$

$$PR = \frac{L_w \cdot \dot{m}_{\text{dist}}}{\dot{Q}_{des}} \quad (2)$$

$$SEC = \frac{\dot{Q}_{des}}{\dot{m}_{\text{dist}}} \quad (3)$$

with

$$\dot{Q}_{\text{cond}} = \dot{m}_{\text{cond}} c_{p,w} \left(T_{\text{cond,in}} - T_{\text{cond,out}}\right) \quad (4)$$

$$\dot{Q}_{\text{des}} = \dot{m}_{\text{des}} c_{p,w} \left(T_{\text{ads,in}} - T_{\text{ads,out}}\right) \quad (5)$$

where $\dot{m}_{des/cond}$ [kg s^{-1}] are the flow rates supplied to the heat exchangers, $c_{p,w}$ is the specific heat capacity [kJ kg^{-1} K^{-1}] and $T_{in/out}$ [K] represents the temperature differences between inlet and outlet of the desorber and condenser heat exchangers respectively.
Given the extremely low regeneration temperatures used, ranging between 303 K (30°C) and 321 K (48°C), a fairer comparison with other desalination technologies (especially with those that are electrically-driven) should be based on exergy instead of energy. The Specific Exergy Consumption (*SExC*) should also be monitored and compared with the minimum Specific Exergy Consumption (*minSExC*) that is the exergy needed to evaporate a unitary amount of water:

$$SExC = SEC \left(1 - \frac{T_{cond}}{T_{bed,ads}}\right) \quad (6)$$

$$minSExC = L_w \left(1 - \frac{T_{cond}}{T_{bed,ads}}\right) \quad (7)$$

where L_w is the latent heat of water at the temperature $T_{bed,ads}$ [K]. This results in the second law efficiency (exergy efficiency):

$$\eta_{2nd\ Law} = \frac{minSExC}{SExC} = \frac{SEC}{L_w} \quad (8)$$

The high values in *SDWP* (24 kg_{water} kg_{ig}^{-1} day^{-1}) and Performance Ratio (*PR*, daily average 0.62, peaking to 0.98) visible in Fig 7 are achieved due to the rapid cycling. The *SEC* ranges most of the time between 693 kWh m_{water}^{-3} and 1511 kWh m_{water}^{-3}, peaking regularly and instantaneously to higher values up to 8590 kWh m_{water}^{-3} at every switch of the two beds. This trend of the *SEC* sets a challenge for the design of beds with super-efficient heat transfer, which can reduce the magnitude of the peaks.
The trend of *SExC* shows minima down to 15 kWh_{ex} m_{water}^{-3} and maxima reaching 435 kWh_{ex} m_{water}^{-3}. The overall dynamics features energy consumption indexes increasing during the daytime. This is because of the decrease of the relative humidity (Fig. 7b) at which the adsorption material operates and the consequent larger enthalpy of adsorption (Fig. 5). Nevertheless, the 2nd law efficiency reach very high values of 0.86 and an average of 0.52. Adsorption desalination is a high exergy efficiency technology, especially when its regeneration, condensing and evaporating temperatures can be kept close each other within a narrow range.

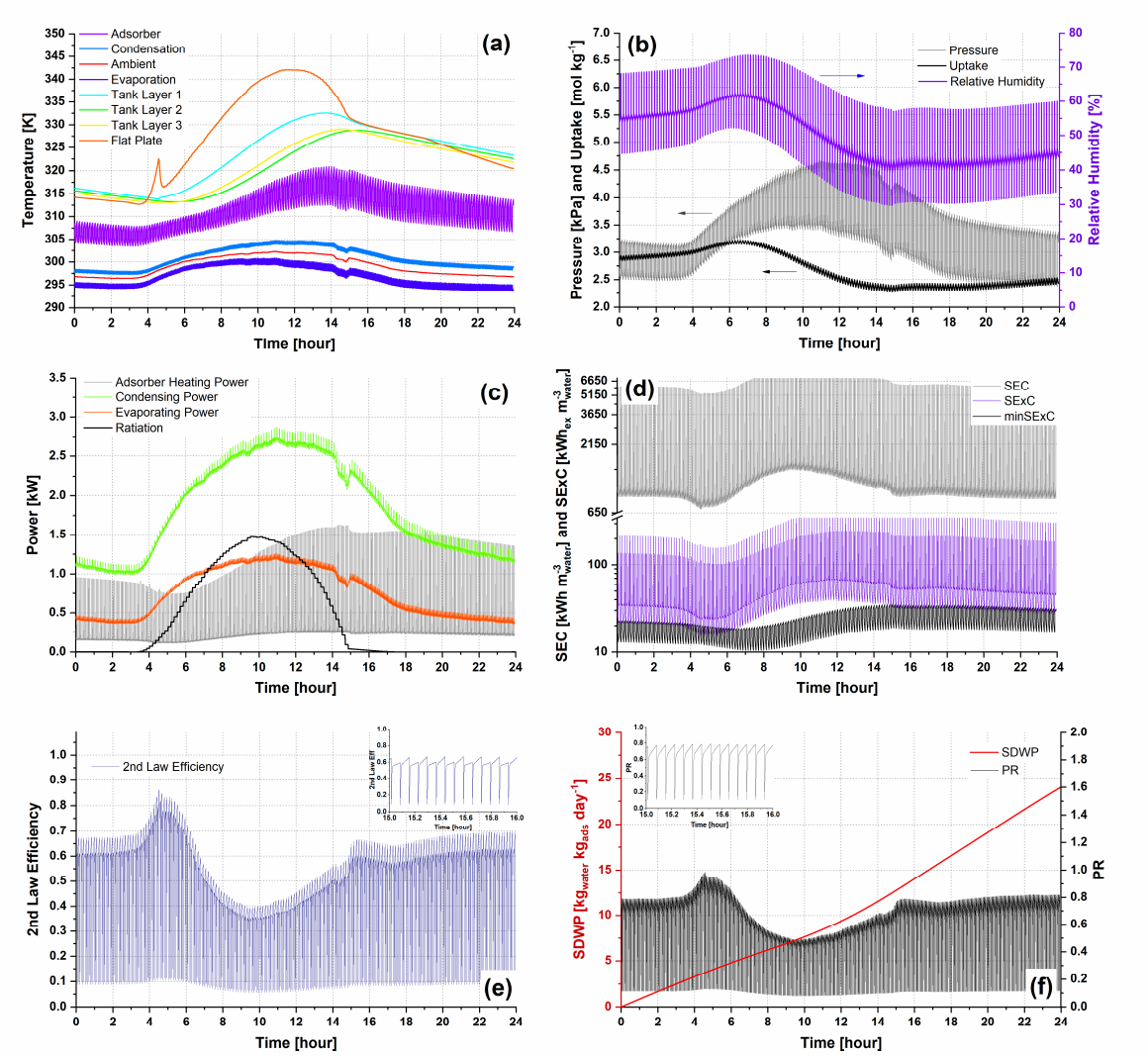

Figure 7: The system's performance during an average summer day in Sicily: (a) The solar tank is split into 3 layers and heated by the radiation of an average day every 24 h. The temperature curves of the system peak in the afternoon and cool down until the early morning. For simplicity, only one adsorber is plotted; (b) Uptake, adsorber pressure and adsorber relative humidity. The adsorber pressure is higher than for pure water due to presence of salted water; (c) System's powers including solar radiation, adsorbers heating power, condensing and evaporating power; (d) Instantaneous Specific Energy Consumption (SEC), Specific Exergy Consumption (SExC) and Thermodynamic Minimum Specific Energy Consumption (minSExC) from the latent heat of water; (e) Second Law Efficiency as the ratio between the Specific Exergy Consumption (SExC) and the Minimum Specific Exergy Consumption (minSExC); (f) Performance Ratio (PR) and cumulative Specific Daily Water Production (SDWP).

5. System scale up

The performance of the solar powered adsorption desalinator was calculated for different sizes of solar collectors. The results in Fig. 8 are based on a plant output of one cubic metre of water per day. In Fig. 8, the simulations were conducted using the heat transfer coefficient U_{fp} = 5.2 W m^{-2} K^{-1} for a vacuum flat plate solar collector presented by Moss et al. [10]. To reduce the computational demand, a heat sink supplies cooling water at constant temperature of 20 °C to the condenser and adsorption beds during adsorption in accordance the experimental datasets used for model validation [22]. In a real system, colder heat sink temperatures would improve the performance. For example, the amount of water produced by silica gel doubles when moving from 5°C to 10°C difference between the regeneration and condensation temperatures [22]. This is a conservative assumption, since the average annual ambient air temperature never exceeded 20°C in the used datasets. The same constant ambient temperature was used to assess heat losses from the solar collector.

The result curves for Messina are very similar for spring, summer and autumn indicating that one system size could provide a constant performance throughout most of the year. For winter, the curve is shifted to the right, requiring a larger system to produce the same amount of water compared to the other three seasons in Messina. The solar collector area in winter would have to be increased by 55 % according to Fig. 8. The curves also reflect a trade-off between the solar collector area and adsorption bed size per cubic metre of water. Larger adsorption beds can produce the same amount of water using less solar collector area and accordingly lower regeneration temperatures. This case could be applied when the solar collector is installed on a confined space like the roof of a residential house. In case the space for the solar field is not constrained, the adsorption system size can be reduced by a larger solar collector field that provides hotter regeneration temperatures.

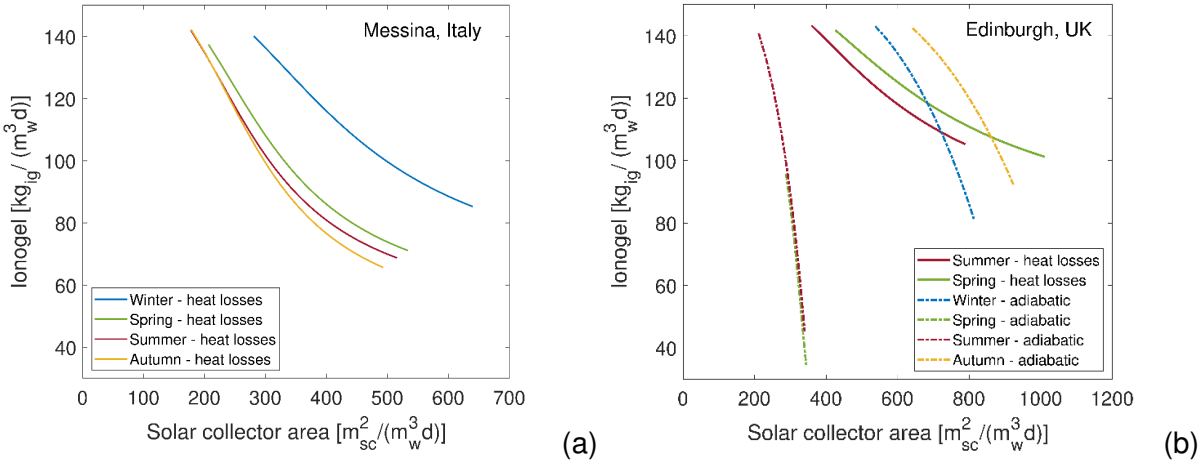

Figure 8: Heat losses of the solar collector impair the system performance: (a) Solar collector with heat losses. (b) Adiabatic solar collector. Example for a system supplying one person with 143 L of water per day.

For the case of Scotland in Fig. 8b, the analysis distinguishes between cases that include heat losses and adiabatic cases. Comparing the cases including heat losses between Messina and Edinburgh, it can be seen that the curves for Edinburgh are shifted to the right. This shift indicates that the solar field in Edinburgh would need to be twice as high as in Messina to supply the same amount of ionogel with sufficient heat to produce the same amount of water. The adiabatic case was introduced for Edinburgh, because heat losses were too high to operate the system in autumn and winter. In winter and autumn, the hours of daylight and solar radiation are insufficient to power the adsorption system when heat losses are considered. Hence, a system in Northern Europe could not operate during this period. The diverging slopes between the adiabatic and heat loss cases for summer and spring in Fig. 7b indicate that heat losses significantly reduce the efficiency of larger solar fields to produce the same amount of water. Heat losses of the solar collector require at least 80 % larger solar collector area to compensate. The adiabatic cases for winter and autumn in Fig. 8b show that solar desalination could be possible during winter with large adsorbers 80-140 kg_{ig} m_{water}^{-3} day^{-1} and 500-900 m_{sc}^2 m_{ig}^{-3} day^{-1}. From Fig. 8, solar powered adsorption desalination appears feasible for Mediterranean countries throughout the year. In Northern Europe, it could be an option for smaller applications in remote areas like the Scottish isles during the dry summer months. Current evacuated flat plate solar collectors provide viable results for Italy today, while advances in the technology will improve the case for the UK. Fig. 8 applies local differences in water consumption to the results. The Italian National Institute of Statistics reports the water consumption in Italy at 241 L per person per day [38], while water consumption in the UK is reported at 143 L per person per day [5]. Hence, water consumption in Italy is 70 % higher than the demand in the UK. Fig 8 applies the water consumption to the results of Fig. 7 for an example solar field of 7000 m_{sc}^2, which is about the size of a football pitch.

The analysis in Fig. 9 assesses different adsorption bed sizes and estimates the number of consumers it can supply with drinking water. It can be seen that the solar radiation in

Edinburgh can only power small systems of 700-2000 kg_{ig}, but given the lower water consumption in the UK, the same system of 2000 kg_{ig} can supply 20 % more consumers in the UK than in Italy. However, stronger solar radiation in Italy allows the operation of up to 5600 kg_{ig} with a solar field of 7000 m_{sc}^2, which allows the supply of 160 consumers in Italy instead of 115 consumers with the largest possible system in the UK for the given solar collector area. Hence, the same solar field can supply 40 % more people in Italy than in the UK. Despite the lower solar radiation in Scotland, it can be more efficient to operate a solar desalination system in the UK than in Italy in some cases, when local water consumption is taken into account. This highlights the importance of water conservation as a first step prior to desalination in water stressed regions. Moreover, high water losses of the public water supply system are another major issue, as the water input is reported at 385 L per person per day in Italy but only 241 L per day per person are delivered [42].

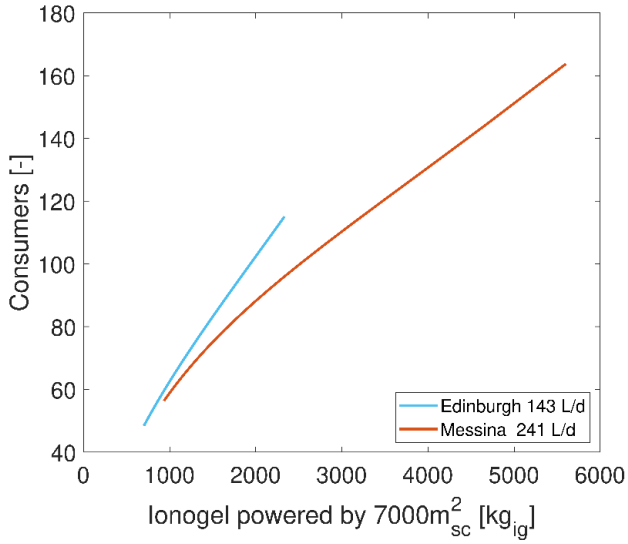

Figure 9: The number of consumers that can be supplied during summer by a 7000 m^2 solar field taking heat losses and regional water consumption into account: Italy: 241 L per person per day [42]. UK: 143 L per person per day [5].

6. Conclusions

In this work, a solar powered adsorption desalinator is introduced in experimentally validated simulations for Northern and Southern Europe. Minute-by-minute solar radiation data for Edinburgh (UK) and Messina (Italy) was processed to obtain average days for each season and to identify the ideal tilting angle for each location. The results were used as heat input for a dynamic adsorption desalination system that was experimentally calibrated using advanced ionogel adsorption material. For the simulations the adsorption desalinator is connected to an evacuated flat plate solar collector field and an insulated hot water tank as sensible heat storage. The results show that heat storage allows the system to operate throughout the night. Moreover, the size of the hot water tank is secondary to the system design, as the impact on the performance is negligible for the range of tank sizes investigated here. The size of the solar field and the adsorption bed were the two key system parameters identified by this analysis. A solar powered adsorption desalinator in Sicily containing five tonnes featuring a 7000 m^2 collector area could provide 160 people with drinking water throughout the year. In Scotland, the proposed system could bring water relief to remote areas during the summer months. Moreover, in some cases solar desalination can be more efficient in the UK than in Italy, when regional water consumption behaviour is taken into account.

Acknowledgments

The authors are grateful to Dr. Rhys Lloyd for his support during the preparation of the manuscript.

Appendix A. Modelling equations

Appendix A.1. Solar radiation

The angular position of the sun at solar noon is known as declination δ and was approximated by Cooper [43]:

$$\delta = 23.45\ sin\left(360\frac{284+n}{365}\right) \quad (A.1)$$

where n represents the n_{th} day with average values of n = 17; 105; 198 and 288 for winter, spring, summer and autumn respectively [39]. The ratio of beam radiation on the tilted surface to the horizontal surface is given by [39]:

$$R_b = \frac{cos(\theta_s)}{cos(\theta_z)} \quad (A.2)$$

With the angle of incidence of beam radiation θ on a surface [39]:

$$sin(\theta_s) = sin(\delta)sin(\varphi)cos(\beta) - sin(\delta)cos(\varphi)sin(\beta)cos(\gamma) + cos(\delta)cos(\varphi)cos(\beta)cos(\omega_s) + cos(\delta)sin(\varphi)sin(\beta)cos(\gamma)cos(\omega_s) + cos(\delta)sin(\beta)sin(\gamma)sin(\omega_s) \quad (A.3)$$

where φ = 55.95° N is the latitude of Edinburgh and φ = 38.19° N is the latitude of Messina. The slope of the tilted surface is represented by β for 0° ≤ β ≤ 90°, γ = 0° for a southward facing tilted plane, ω_s is the hour angle due to rotation of the earth of 15° per hour, ω_s = 0° at noon, morning negative and afternoon positive [39]. The zenith angle θ_z between the vertical and the line to the sun is described by [39]:

$$cos(\theta_z) = cos(\varphi)cos(\theta)cos(\omega_s) + sin(\varphi)sin(\delta) \quad (A.4)$$

The solar azimuth angle describes the deviation of the sun's projection on a horizontal plane from south [39]:

$$\gamma_s = sign(\omega_s)\left[cos^{-1}\left(\frac{cos(\theta_z)sin(\varphi)-sin(\delta)}{sin(\theta_z)cos(\varphi)}\right)\right] \quad (A.5)$$

The sunset hour ω_{ss} angle is described by [39]:

$$cos(\omega_{ss}) = \frac{sin(\varphi)sin(\delta)}{cos(\varphi)cos(\delta)} \quad (A.6)$$

The number of daylight hours N_{dlh} can be calculated from angle is described by [39]:

$$N_{dlh} = \frac{2}{15}cos^{-1}\left(-tan(\varphi)tan(\delta)\right) \quad (A.7)$$

The total solar radiation on the tilted surface I_T can be expressed by [44]:

$$I_T = I_b R_b + I_d\left(\frac{1+cos(\beta)}{2}\right) + I\rho_g\left(\frac{1-cos(\beta)}{2}\right) \quad (A.8)$$

where ρ_g is the reflectance of the ground for solar radiation, which was assumed at 0.40 [44], I_b the beam radiation on the horizontal plane [W m^{-2}], I_d the diffuse radiation on the horizontal plane [W m^{-2}] and I the global radiation on the horizontal plane [W m^{-2}].

Appendix A.2. Solar tank

The outlet temperatures of all heat exchangers is given by the logarithmic mean temperature difference:

$$T_{\text{out}} = T + (T_{\text{in}} - T)exp\left(\frac{-UA}{\dot{m}c_{p,w}}\right) \quad (A.9)$$

where U is the overall heat transfer coefficient [W m^{-2} K^{-1}], T is the temperature inside the vessel [K], A is the surface area of the heat exchanger [m^2] and $\dot{m}_{hx}$ is the flow rate of water supplied to the heat exchanger [kg s^{-1}]. The model uses U = 500 W m^{-2} K^{-1} as overall heat transfer coefficient between water and solar absorption plate. The temperature of the flat plate aluminium solar absorption plate is calculated from:

$$M_{hx,fp}c_{p,hx}\frac{dT_{fp}}{dt} = \eta_{sc}I_t A_{sc} + \dot{m}_{sol}c_{p,w}\left(T_{sc,in} - T_{sc,out}\right) - U_{fp,amb}A_{fp,amb}\left(T_{fp} - T_{amb}\right) \quad (A.10)$$

the heat transfer coefficient of the flat plate solar collector $U_{fp,amb}$ is 5.2 W m^{-2} K^{-1} as reported by Moss et al. for an evacuated flat plate solar collectors [10]. The temperatures of the three water layers within the solar tank are:

$$V_{\text{lay1}} c_{p,w} \rho \frac{dT_{\text{lay1}}}{dt} = m_{\text{sol}} c_{p,w} \left(T_{\text{sc,out}} - T_{sc,\text{in}}\right) + m_{\text{heat}} c_{p,w} \left(T_{\text{lay2}} - T_{\text{lay1}}\right) + U_{\text{lay}} A_{\text{lay}} \left(T_{\text{lay2}} - T_{\text{lay1}}\right) \quad \text{(A.11)}$$

$$V_{\text{lay3}} c_{p,w} \rho \frac{dT_{\text{lay2}}}{dt} = m_{\text{heat}} c_{p,w} \left(T_{\text{lay3}} - T_{\text{lay2}}\right) + U_{\text{lay}} A_{\text{lay}} \left[\left(T_{\text{lay3}} - T_{\text{lay2}}\right) + \left(T_{\text{lay1}} - T_{\text{lay2}}\right)\right] \quad \text{(A.12)}$$

$$V_{\text{lay3}} c_{p,w} \rho \frac{dT_{\text{lay3}}}{dt} = U_{\text{lay}} A_{\text{lay}} \left(T_{\text{lay2}} - T_{\text{lay3}}\right) + m_{\text{heat}} c_{p,w} \left(T_{\text{heat,out}} - T_{\text{lay3}}\right) \quad \text{(A.13)}$$

where $T_{lay1} = T_{heat,in}$.

Appendix A.3. Adsorption desalination

A lumped parameter dynamic adsorption desalination model [26,45] was adapted and validated by experimental data [22]. Table A.2 shows sequence parameters used to adjust the modelling equations for each phase of the adsorption cycle [37]. All parameters used in the model are given in table A.3.

Table A.2: Modelling parameters for the adsorption cycle sequence

Phase	Cycle	Bed 1	τ_1	τ_2	ω
I	1-2	Isosteric Heating	0	0	0
II	2-3	Desorption	1	0	1
III	3-4	Isosoteric Cooling	0	0	0
VI	4-1	Adsorption	0	1	1

The water uptake of the adsorption material is assessed by Dubinin-Astakhov (DA) isotherms [46,47]:

$$q^* = q_0 \exp\left(-\left[\frac{RT}{E} \ln\left(\frac{p_{\text{sat}}}{p}\right)\right]^{n_{DA}}\right) \quad \text{(A.14)}$$

where q_0 [kg$_{\text{water}}$ kg$_{\text{sorbent}}^{-1}$] is the saturation uptake, E [kJ kg^{-1}] and n_{DA} [-] are DA parameters [31], R the ideal gas constant [J mol^{-1} K^{-1}] and the saturation pressure of water p_{sat} [bar], which is calculated through the Antoine equation $log_{10}(p_{sat}) = 4.6543 - (1435.264/(T-64.848))$ [48] by using the temperature T in [K]. The pressure p is also calculated from the Antoine equation during desorption, while it is derived from the Pitzer model [41,49] during adsorption to account for the presence of seawater in the evaporator as described in [38]. The sorption kinetics are assessed by the linear driving force (LDF) equation:

$$\frac{dq_{1/2}}{dt} = \omega_{1/2} k_{ldf} (q^* - q) \quad \text{(A.15)}$$

The mass balances of the condenser and evaporator are shown below:

$$\frac{dM_{sw,\text{evap}}}{dt} = -M_{ig} \left(\tau_1 \frac{dq_1}{dt} + \tau_2 \frac{dq_2}{dt}\right) + \dot{m}_{sw,\text{in}} - \dot{m}_{sw,\text{out}} \quad \text{(A.16)}$$

$$\frac{dM_{w,\text{cond}}}{dt} = M_{ig} \left(\tau_2 \frac{dq_1}{dt} + \tau_1 \frac{dq_2}{dt}\right) - \dot{m}_{\text{dist}} \quad \text{(A.17)}$$

The energy balance for the evaporator is:

$$\left(M_{hx,\text{evap}} c_{p,hx} + M_{sw,\text{evap}} c_{p,sw}\right) \frac{dT_{\text{evap}}}{dt} = \left(\tau_1 \frac{dq_1}{dt} + \tau_2 \frac{dq_2}{dt}\right) M_{ig} L_w + \dot{m}_{\text{evap}} c_{p,w} \left(T_{\text{evap,in}} - T_{\text{evap,out}}\right) \quad \text{(A.18)}$$

where $M_{hx,evap}$ is the mass of the heat exchanger [kg], the flow rate F [kg s^{-1}], the latent heat L of water [kJ kg^{-1}], $c_{p,hx}$ is the specific heat of the aluminium heat exchanger [kJ kg^{-1} K^{-1}] and $c_{p,w}$ is the specific eat of the cooling water [kJ kg^{-1} K^{-1}]. The specific heat of seawater $c_{p,sw}$ inside the evaporation vessel is 3.9 kJ kg^{-1} K^{-1} for seawater at ambient temperature [50]. The energy balance of the condenser is:

$$\left(M_{hx,cond}c_{p,hx} + M_{w,cond}c_{p,w,cond}\right)\frac{dT_{cond}}{dt} = \left(\tau_2\frac{dq_1}{dt} + \tau_1\frac{dq_2}{dt}\right)M_{ig}L_w + \dot{m}_{cond}c_{p,w}\left(T_{cond,in} - T_{cond,out}\right) \quad \text{(A.19)}$$

The energy balances for the adsorbers are split between the heat exchangers and the adsorption material:

$$M_{hx,ads}c_{p,hx}\frac{dT_{hx,ads}}{dt} = \dot{m}_{ads}c_{p,w}\left(T_{ads,in} - T_{ads,out}\right) + UA_{hx}\left(T_{bed} - T_{hx,ads}\right) \quad \text{(A.20)}$$

$$\left(M_{ig}c_{p,ig} + M_{w,ig,ads}c_{p,w,ads}\right)\frac{dT_{bed,ads}}{dt} = \Delta h_{ads}M_{ig}\frac{dq}{dt} + UA_{ads}\left(T_{hx,ads} - T_{bed,ads}\right) \quad \text{(A.21)}$$

All outlet temperatures $T_{i,out}$ [K] are determined by the logarithmic mean temperature difference given in eq. (A.9). The heat of adsorption, Δh_{ig} [kJ kg^{-1}] is derived from Clausius-Clapeyron and the DA isotherm [51], where $\theta = (q/q_0)$:

$$\Delta h_{ig} = L_w + E\ln\left(\frac{1}{\Theta}\right)^{1/n_{DA}} + \frac{E\alpha T}{n_{DA}}\left(\frac{1}{\Theta}\right)^{-(n_{DA}-1)/n_{DA}} \quad \text{(A.22)}$$

Table A.3: Simulation parameters used in this study for the small-scale adsorption desalinator [36].

Property	Unit	Value	Reference
η_{sc}	--	0.8	[26]
A_{sc}	m^2	2	assumed
$\dot{m}_{evap}$	L min^{-1}	2.1	assumed
$\dot{m}_{cond}$	L min^{-1}	4	assumed
$\dot{m}_{ads/des}$	L min^{-1}	1.5	assumed
k_{ldf}	s^{-1}	0.9	assumed
$M_{hx,evap}\ c_{p,hx}$	kJ K^{-1}	0.137	assumed
$M_{hx,cond}\ c_{p,hx}$	kJ K^{-1}	0.378	assumed
$M_{hx,ads}\ c_{p,hx,ads}$	kJ K^{-1}	0.546	assumed
$M_{hx,fp}\ c_{p,hx}$	kJ K^{-1}	20.25	[26]
$U_{lay}A_{lay}$	W K^{-1}	10	[26]
UA_{hx}	W K^{-1}	90	this study*
UA_{ads}	W K^{-1}	30	this study*
UA_{cond}	W K^{-1}	90	this study*
UA_{evap}	W K^{-1}	70	this study*
t_{cycle}	s	500	[22]
R_p	m	0.002	[22]
M_{ad}	kg	0.2	[36]
$c_{p,ad}$	kJ kg^{-1}K^{-1}	1	[52]
q_0	kg kg^{-1}	32.2	[22]
E	kJ kg^{-1}	1.04	[22]
n_{DA}	-	0.2	[22]
R	J mol^{-1}K^{-1}	8.314	

Note: *The heat transfer parameters *UA* are fitted to experimental results as part of this study

Nomenclature

Greek

α	Thermal expansion coefficient (K^{-1})
β	Slope of the tilted surface (deg)
Δh_{ads}	Heat of adsorption (kJ kg_w^{-1})
δ	Angular position of the sun
η	Efficiency
γ_s	Azimuth angle (deg)
ω	Modelling parameter (-)
ω_S	Sun hour angle (deg)
φ	Latitude (deg)
ρ_g	Ground reflectance
τ	Modelling parameter (-)
θ	Normalised adsorption uptake
θ_s	Incidence angle (deg)
θ_z	Zenith angle (deg)
ξ	Modelling parameter

Roman

A	Heat exchanger area (m^2)
c_p	Specific heat (kJ kg^{-1} K^{-1})
D_{s0}	Kinetic constant (m^2 s^{-1})
E	DA parameter (kJ kg^{-1})
E_a	Activation energy (kJ kg^{-1})
I	Radiation (W m^{-2})
k_{ldf}	Lumped parameter LDF model (1 s^{-1})
L	Latent heat (kJ kg^{-1})
M	Mass (kg)
n	Number
N_C	Number of cycles performed within one day (-)
n_{DA}	DA exponent (-)
N_{dlh}	Number of daylight hours
p	pressure (bar)
Q	Heat (kJ)
q	Water vapour uptake of the adsorption material (kg kg^{-1})
q_0	Saturation uptake (kg kg^{-1})
R	Real gas constant (J mol^{-1} K^{-1})
R_b	Radiation factor
R_p	Pellet radius (mm)
T	Temperature (K)
t	Time (s)
U	Overall Heat transfer coefficient (W m^{-2} K^{-1})
$\dot{m}$	Water flow rate supplied to heat ex- changer (kg s^{-1})
$\dot{Q}$	Heat flow (kJ s^{-1})

Subscripts

ads	Adsorber
amb	Ambient
b	Beam
cond	Condenser
cycle	Adsorption cycle
d	Diffuse
des	Desorber
dist	Distillate

el	Electricity
evap	Evaporator
fp	Flat plate
hx	Heat exchanger
ig	Ionogel
lay	Solar tank layer
sat	Saturation conditions
sc	Solar collector
sg	Silica gel
ss	Sunset
sw	Seawater
T	Total
th	Thermal
vap	Vapour
w	Water

Acronyms

MED	Multi effect distillation
MSF	Multi stage flash
minSExC	Thermodynamic Minimum Specific Exergy Consumption ($kWh_{ex}\ m_{water}^{-3}$)
PR	Performance Ratio
RH	Relative humidity (%)
SEC	Specific Energy Consumption ($kWh\ m_{water}^{-3}$)
SExC	Specific Exergy Consumption ($kWh_{ex}\ m_{water}^{-3}$)
SDWP	Specific Daily Water Production ($kg_{water}\ kg_{sorbent}^{-1}\ day^{-1}$)

References

[1] Marsh T, Cole G, Wilby R. Major droughts in England and Wales, 1800-2006. Weather 2007;62:87–93. doi:10.1002/wea.67.

[2] Water situation reports for England - GOV.UK n.d. https://www.gov.uk/government/collections/water-situation-reports-for-england (accessed January 3, 2021).

[3] Orth R, Zscheischler J, Seneviratne SI. Record dry summer in 2015 challenges precipitation projections in Central Europe. Sci Rep 2016;6:1–8. doi:10.1038/srep28334.

[4] Pedro-Monzonís M, Solera A, Ferrer J, Estrela T, Paredes-Arquiola J. A review of water scarcity and drought indexes in water resources planning and management. J Hydrol 2015;527:482–93. doi:10.1016/j.jhydrol.2015.05.003.

[5] Water supply and demand management - National Audit Office (NAO) Report n.d. https://www.nao.org.uk/report/water-supply-and-demand-management/ (accessed January 3, 2021).

[6] Majid A, Cardenes I, Zorn C, Russell T, Colquhoun K, Bañares-Alcantara R, et al. An Analysis of Electricity Consumption Patterns in the Water and Wastewater Sectors in South East England, UK. Water 2020;12:225. doi:10.3390/w12010225.

[7] Greenhouse gas reporting: conversion factors 2019 - GOV.UK n.d. https://www.gov.uk/government/publications/greenhouse-gas-reporting-conversion-factors-2019 (accessed February 16, 2021).

[8] Ali MT, Fath HES, Armstrong PR. A comprehensive techno-economical review of indirect solar desalination. Renew Sustain Energy Rev 2011;15:4187–99. doi:10.1016/j.rser.2011.05.012.

[9] Leblebici SY, Leppert L, Li Y, Reyes-Lillo SE, Wickenburg S, Wong E, et al. Facet-dependent photovoltaic efficiency variations in single grains of hybrid halide perovskite. Nat Energy 2016;1:1–7. doi:10.1038/nenergy.2016.93.

[10] Moss RW, Henshall P, Arya F, Shire GSF, Hyde T, Eames PC. Performance and operational effectiveness of evacuated flat plate solar collectors compared with conventional thermal, PVT and PV panels. Appl Energy 2018;216:588–601. doi:10.1016/j.apenergy.2018.01.001.

[11] Palenzuela P, Zaragoza G, Alarcón-Padilla DC. Characterisation of the coupling of multi-effect distillation plants toconcentrating solar power plants. Energy 2015;82:986–95. doi:10.1016/j.energy.2015.01.109.

[12] Shahzad MW, Burhan M, Ang L, Ng KC. Energy-water-environment nexus underpinning future desalination sustainability. Desalination 2017;413:52–64. doi:10.1016/j.desal.2017.03.009.

[13] Wang Z, Horseman T, Straub AP, Yip NY, Li D, Elimelech M, et al. Pathways and challenges for efficient solar-thermal desalination. Sci Adv 2019;5:eaax0763. doi:10.1126/sciadv.aax0763.

[14] Al-Karaghouli A, Kazmerski LL. Energy consumption and water production cost of conventional and renewable-energy-powered desalination processes. Renew Sustain Energy Rev 2013;24:343–56. doi:10.1016/j.rser.2012.12.064.

[15] El-Nashar AM, Samad M. The solar desalination plant in Abu Dhabi: 13 years of performance and operation history. Renew Energy 1998;14:263–74. doi:10.1016/S0960-1481(98)00076-7.

[16] Moustafa SMA, Jarrar DI, El-Mansy HI. Performance of a self-regulating solar multistage flash desalination system. Sol Energy 1985;35:333–40. doi:10.1016/0038-092X(85)90141-0.

[17] Ng KC, Thu K, Kim Y, Chakraborty A, Amy G. Adsorption desalination: An emerging low-cost thermal desalination method. Desalination 2013;308:161–79. doi:10.1016/J.DESAL.2012.07.030.

[18] Youssef PG, Dakkama H, Mahmoud SM, AL-Dadah RK. Experimental investigation of adsorption water desalination/cooling system using CPO-27Ni MOF. Desalination 2017;404:192–9. doi:10.1016/j.desal.2016.11.008.

[19] Sapienza A, Palomba V, Gullì G, Frazzica A, Vasta S. A new management strategy based on the reallocation of ads-/desorption times: Experimental operation of a full-scale 3 beds adsorption chiller. Appl Energy 2017;205:1081–90. doi:10.1016/j.apenergy.2017.08.036.
[20] Sapienza A, Santamaria S, Frazzica A, Freni A. Influence of the management strategy and operating conditions on the performance of an adsorption chiller. Energy 2011;36:5532–8. doi:10.1016/j.energy.2011.07.020.
[21] Askalany AA, Freni A, Santori G. Supported ionic liquid water sorbent for high throughput desalination and drying. Desalination 2019;452:258–64. doi:10.1016/J.DESAL.2018.11.002.
[22] Olkis C, Dong H, Brandani S, Santori G. Ionogels at the Water-Energy Nexus for Desalination Powered by Ultralow-Grade Heat. Environ Sci Technol 2020;54:3591–8. doi:10.1021/acs.est.9b06037.
[23] Son HS, Shahzad MW, Ghaffour N, Ng KC. Pilot studies on synergetic impacts of energy utilization in hybrid desalination system: Multi-effect distillation and adsorption cycle (MED-AD). Desalination 2020;477:114266. doi:10.1016/j.desal.2019.114266.
[24] Wang RZ, Li M, Xu YX, Wu JY. An energy efficient hybrid system of solar powered water heater and adsorption ice maker. Sol Energy 2000;68:189–95. doi:10.1016/S0038-092X(99)00062-6.
[25] Freni A, Maggio G, Vasta S, Santori G, Polonara F, Restuccia G. Optimization of a solar-powered adsorptive ice-maker by a mathematical method. Sol Energy 2008;82. doi:10.1016/j.solener.2008.05.002.
[26] Santori G, Sapienza A, Freni A. A dynamic multi-level model for adsorptive solar cooling. Renew Energy 2012;43:301–12. doi:10.1016/j.renene.2011.11.039.
[27] Gibelhaus A, Tangkrachang T, Bau U, Seiler J, Bardow A. Integrated design and control of full sorption chiller systems. Energy 2019;185:409–22. doi:10.1016/j.energy.2019.06.169.
[28] Clausse M, Alam KCA, Meunier F. Residential air conditioning and heating by means of enhanced solar collectors coupled to an adsorption system. Sol Energy 2008;82:885–92. doi:10.1016/j.solener.2008.04.001.
[29] Palomba V, Vasta S, Freni A, Pan Q, Wang R, Zhai X. Increasing the share of renewables through adsorption solar cooling: A validated case study. Renew Energy 2017;110:126–40. doi:10.1016/j.renene.2016.12.016.
[30] Alsaman AS, Askalany AA, Harby K, Ahmed MS. Performance evaluation of a solar-driven adsorption desalination-cooling system. Energy 2017;128:196–207. doi:10.1016/j.energy.2017.04.010.
[31] Kim YD, Thu K, Masry ME, Ng KC. Water quality assessment of solar-assisted adsorption desalination cycle. Desalination 2014;344:144–51. doi:10.1016/j.desal.2014.03.021.
[32] Du B, Gao J, Zeng L, Su X, Zhang X, Yu S, et al. Area optimization of solar collectors for adsorption desalination. Sol Energy 2017;157:298–308. doi:10.1016/j.solener.2017.08.032.
[33] Elsayed E, AL-Dadah R, Mahmoud S, Anderson P, Elsayed A. Experimental testing of aluminium fumarate MOF for adsorption desalination. Desalination 2020;475:114170. doi:10.1016/j.desal.2019.114170.
[34] Askalany A, Olkis C, Bramanti E, Lapshin D, Calabrese L, Proverbio E, et al. Silica-Supported Ionic Liquids for Heat-Powered Sorption Desalination. ACS Appl Mater Interfaces 2019;11:36497–505. doi:10.1021/acsami.9b07602.
[35] Dong H, Askalany AA, Olkis C, Zhao J, Santori G. Hydrothermal stability of water sorption ionogels. Energy 2019;189:116186. doi:10.1016/j.energy.2019.116186.
[36] Olkis C, Brandani S, Santori G. Design and experimental study of a small scale adsorption desalinator. Appl Energy 2019;253:113584. doi:10.1016/j.apenergy.2019.113584.
[37] Olkis C, Brandani S, Santori G. Cycle and performance analysis of a small-scale adsorption heat transformer for desalination and cooling applications. Chem Eng J

2019;378:122104. doi:10.1016/j.cej.2019.122104.
[38] Olkis C, Santori G, Brandani S. An Adsorption Reverse Electrodialysis system for the generation of electricity from low-grade heat. Appl Energy 2018;231:222–34. doi:10.1016/J.APENERGY.2018.09.112.
[39] Duffie JA, Beckman WA. Solar Engineering of Thermal Processes: Fourth Edition. 2013. doi:10.1002/9781118671603.
[40] Chang TP. The Sun's apparent position and the optimal tilt angle of a solar collector in the northern hemisphere. Sol Energy 2009;83:1274–84. doi:10.1016/j.solener.2009.02.009.
[41] Giacalone F, Olkis C, Santori G, Cipollina A, Brandani S, Micale G. Novel solutions for closed-loop reverse electrodialysis: Thermodynamic characterisation and perspective analysis. Energy 2019;166:674–89. doi:10.1016/j.energy.2018.10.049.
[42] Censimento delle acque per uso civile n.d. https://www.istat.it/it/archivio/207497 (accessed January 3, 2021).
[43] Cooper PI. The absorption of radiation in solar stills. Sol Energy 1969;12:333–46. doi:10.1016/0038-092X(69)90047-4.
[44] Liu BYH, Liu BYH, Jordan RC. A rational procedure for predicting the long-term average performance of flat-plate solar-energy collectors. Sol ENERGY 1963.
[45] Thu K, Yanagi H, Saha BB, Ng KC. Performance investigation on a 4-bed adsorption desalination cycle with internal heat recovery scheme. Desalination 2017;402:88–96. doi:10.1016/j.desal.2016.09.027.
[46] Dubinin MM, Astakhov VA. Development of the concepts of volume filling of micropores in the adsorption of gases and vapors by microporous adsorbents - Communication 1. Carbon adsorbents. Bull Acad Sci USSR Div Chem Sci 1971;20:3–7. doi:10.1007/BF00849307.
[47] Santori G, Di Santis C. Optimal fluids for adsorptive cooling and heating. Sustain Mater Technol 2017;12. doi:10.1016/j.susmat.2017.04.005.
[48] Stull DR. Vapor Pressure of Pure Substances. Organic and Inorganic Compounds. Ind Eng Chem 1947;39:517–40. doi:10.1021/ie50448a022.
[49] Pitzer KS, Mayorga G. Thermodynamics of electrolytes. II. Activity and osmotic coefficients for strong electrolytes with one or both ions univalent. J Phys Chem 1973;77:2300–8. doi:10.1021/j100638a009.
[50] Archer DG, Carter RW. Thermodynamic properties of the NaCl + H2O system. 4. Heat capacities of H2O and NaCl(aq) in cold-stable and supercooled states. J Phys Chem B 2000;104:8563–84. doi:10.1021/jp0003914.
[51] Do DD. Adsorption Analysis: Equilibria and Kinetics. vol. 2. PUBLISHED BY IMPERIAL COLLEGE PRESS AND DISTRIBUTED BY WORLD SCIENTIFIC PUBLISHING CO.; 1998. doi:10.1142/p111.
[52] Brandani S, Cavalcante C, Guimarães A, Ruthven D. Heat Effects in ZLC Experiments. Adsorption 1998;4:275–85. doi:10.1023/a:1008837801299.